Velocity field decomposition in 3D numerical simulations of solar turbulent convection

By D. Georgobiani, N.N. Mansour, A.G. Kosovichev †, R.F. Stein ‡ AND Å. Nordlund ¶

1. Motivation and objectives

Recent achievements in helioseismic observations, in particular, ground-based GONG (Hill *et al.* 1994) and space mission SOHO/MDI (Scherrer *et al.* 1995), provide large amounts of data about the structure and dynamics of the Sun. These data impose observational constraints on numerical and analytical models of turbulent convection, differential rotation, large-scale circulation etc., therefore serving a purpose of testing and calibrating these models. In turn, these models are important for explaining the exciting helioseismic observations and predicting new effects. Therefore it is important to develop the most accurate and realistic models of solar convection and oscillations in order to obtain a clarified picture of the excitation of solar oscillations by turbulent convection and the interaction between turbulence and oscillations on the Sun. These models can be applied to other stars and provide predictions of properties of stellar oscillations, which are important for planned NASA asteroseismology space missions, or to the data from the Kepler mission (Borucki *et al.* 2003).

Realistic 3D numerical models represent a powerful tool for this investigation, because they do not suffer from simplifying assumptions and free parameters common for their analytical counterparts, yet they render the underlying physical picture of a phenomenon rather tractable. We pursue several goals while implementing numerical models. One of the aspects of our investigation is to use realistic simulations of the convective zone to better understand the interactions between mean flow fields, turbulence and acoustics.

Three-dimensional time dependent simulations of solar convection are becoming increasingly more realistic. Simulations of the shallow upper layer of the solar convection zone by Stein & Nordlund (cf Stein & Nordlund (2000) and references therein) demonstrate excellent agreement with existing analytical theories and observations. For instance, there is a remarkable correspondence between the simulated and observed profiles of weak and intermediate strength photospheric FeI and FeII lines (Asplund *et al.* 2000a, Asplund *et al.* 2000b); also, comparison of oscillation spectra in the simulated and solar data from SOHO/MDI by Georgobiani *et al.* (2004), as well as the rates of stochastic energy input to the low-degree solar modes in the simulations and GOLF observations (Roca Cortes *et al.* 1999) show a good agreement (see Stein & Nordlund (2001), Fig 7).

The goal of this paper is to develop a technique for decomposing the simulated turbulent velocity field into its potential and rotational components. According to the fundamental theorem of vector analysis, any well-behaved vector field has a unique representa-

† Hansen Experimental Physics Laboratory, Stanford University, Stanford, CA 94305, USA
‡ Department of Physics and Astronomy, Michigan State University, Lansing, MI 48824, USA
¶ Niels Bohr Institute for Astronomy, Physics and Geophysics, Juliane Maries Vej 30, DK–2100 Copenhagen, Denmark

tion, to within constant vectors, as a sum of a potential field and a solenoidal (rotational) field,

$$\vec{V} = \vec{V}_P + \vec{V}_R, \tag{1.1}$$

where

$$\vec{V}_P = \nabla\phi, \qquad \vec{V}_R = \nabla \times \vec{\psi}. \tag{1.2}$$

For these fields, the following relations hold by definition:

$$\nabla \times \vec{V}_P = 0, \qquad \nabla \cdot \vec{V}_P = \nabla \cdot \vec{V}; \qquad \nabla \cdot \vec{V}_R = 0, \qquad \nabla \times \vec{V}_R = \nabla \times \vec{V}. \tag{1.3}$$

Roughly speaking, all sources and sinks of a given field $\vec{V}$ are collected in $\vec{V}_P$, whereas all its vortices appear in $\vec{V}_R$. This formalism, also called the Helmholtz-Hodge decomposition, is widely used in computational fluid dynamics, because it helps to better visualize complex flows, to recognize their important features, to describe vector fields and study their topology; but it has never been applied before to the 3D numerical simulations of solar convection.

We use flow fields from the 3D hydrodynamic code by Stein & Nordlund for our example of separation of the mean field into the rotational and potential components (see Nordlund & Stein (1990), Stein & Nordlund (2000) and references therein).

2. Vorticity and divergence

In an attempt to decouple turbulent and acoustic components, we look at two characteristics of the mean velocity field - its vorticity and divergence - in the data obtained with the numerical simulations of Stein & Nordlund. Vorticity $|\vec{\omega}| = |\nabla \times \vec{u}|$ is concentrated primarily in strong, fast, turbulent downdrafts, formed in intergranular lanes, whereas flow divergence $d = \nabla \cdot \vec{u}$ is predominantly concentrated in smooth, slow, laminar upflows.

Recent theories, supported by observations, suggest that excitation of solar oscillations originates in the intergranular lines where turbulent motions are particularly strong. As a first step towards a separation of the acoustic signal from turbulence, we look at the temporal power spectra of simulated horizontally averaged vertical velocity u_z, divergence d and enstrophy $|\omega^2|$ signals (Fig 1). The divergence signal shows prominent resonant acoustic modes. It is very similar to the vertical velocity spectrum, but somewhat flatter at higher frequencies. Enstrophy contains mostly background stochastic component, with no resonant modes, except for the first mode peak. This suggests some nonlinear coupling between the divergence and vorticity signals at a particular frequency.

3. Velocity field decomposition

Without loss of generality, we can split the mean velocity field into a potential and rotational components:

$$u_i = \epsilon_{ijk}\psi_{k,j} + \phi_{,i} = u_i^R + u_i^P \tag{3.1}$$

We take divergence of the above, getting:

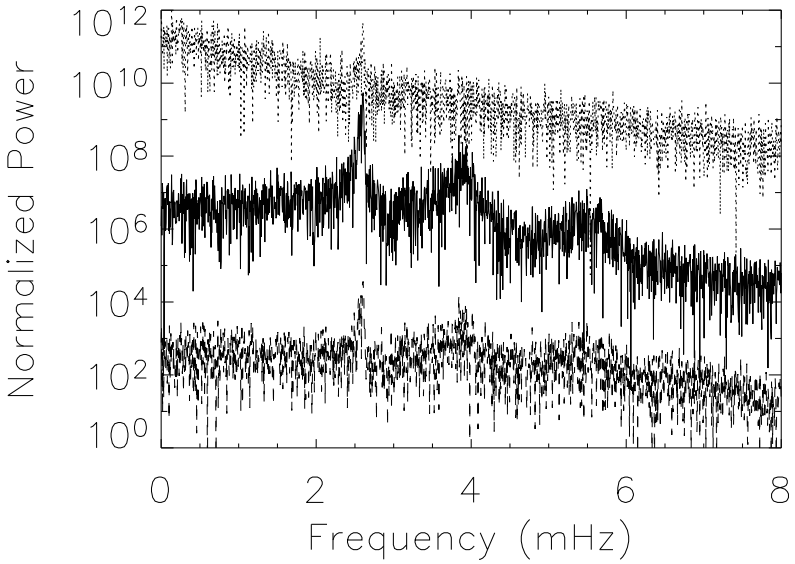

FIGURE 1. Normalized power spectra of radial modes in velocity (solid line), its divergence (dashed line) and enstrophy (dotted line), scaled arbitrarily to facilitate feature recognition. Divergence profile is similar to velocity, although it is flatter at higher frequencies. Enstrophy shows mostly the background noise, with weak first mode.

$$\phi_{,ii} = u_{i,i} = u^P_{i,i} \tag{3.2}$$

and then solve the resulting Poisson equation to obtain the potential velocity component. Then, the rotational component is calculated as a difference between the total velocity and its potential component.

We apply this decomposition to the simulated velocity field. Examples of the potential and rotational components of the flow field are shown as vertical slices through the simulation domain in Fig 2 and as horizontal slices in Fig 3. The total and the rotational velocity slices closely resemble each other visually, therefore we do not present the total velocity pictures. From this, one can conclude that the rotational velocity component is dominant, whereas the potential component is rather weak and featureless. This conclusion is reinforced by the comparison of spatial energy spectra of the three velocity components (Fig 4): the energy content is much lower in the potential velocity component, and it peaks at lower spatial wavenumber (larger characteristic spatial scale) than the vortical (or total) velocity with its dominant sharp small-scale turbulent features. We study different aspects of the velocity decomposition, for instance, temporal power spectra of different components. Our results show that the potential velocity component displays prominent acoustic modes, whereas the rotational component mostly contributes to the characteristic slope of the background noise, with no mode signal (Fig 5). In the last picture, we plot nonradial power spectra, because the horizontally averaged (radial) rotational velocity component is zero.

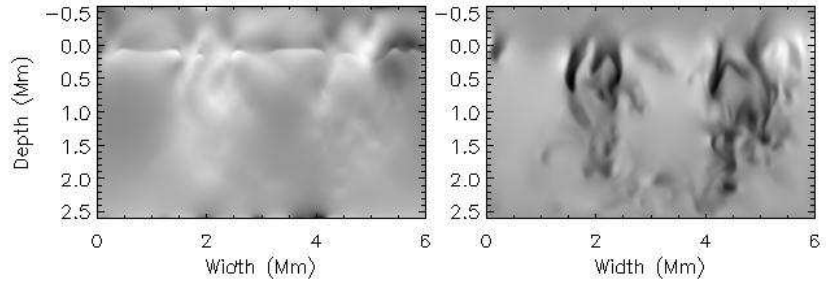

FIGURE 2. Vertical slices of the potential velocity (left panel) and the rotational velocity (right panel) at a fixed arbitrary horizontal coordinate. Potential component looks structureless, while rotational component, similarly to the total velocity, shows strong turbulent downdrafts. The magnitudes change from smallest (light) to largest (dark).

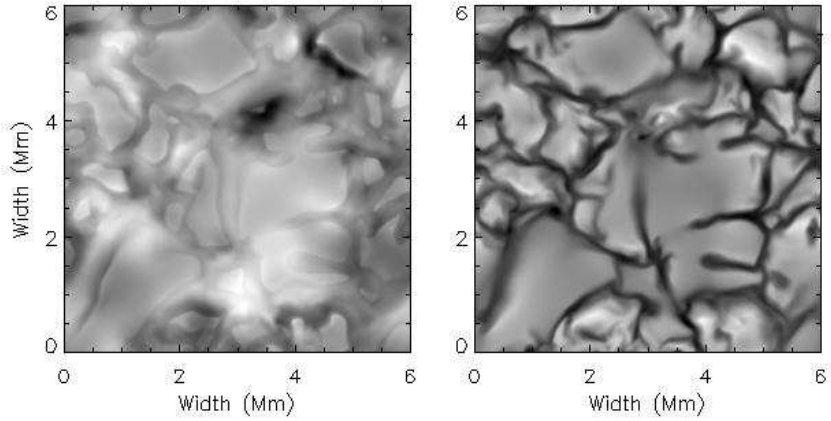

FIGURE 3. Horizontal slices of the potential velocity (left panel) and the rotational velocity (right panel) at the visible surface. There are no sharp features in the potential component, while the rotational component, like the total velocity, exhibits sharp intergranular turbulent features. Black is for largest, white is for smallest magnitudes.

4. Summary and future plans

We have simulated the turbulent velocity field of solar convection using Stein & Nordlund 3D code, and decomposed it into a potential and a rotational component. We have analyzed spatial and temporal spectra of these components. We have found that the kinetic energy content is higher in the rotational velocity component, and that the potential component can be treated as a small perturbation of the total flow field, in agreement with earlier findings (cf Nordlund & Stein 2001). The temporal power spectrum of the potential component shows distinct acoustic mode peaks, while the rotational component spectrum primarily consists of convective background noise, dominating at very low frequencies and quickly decaying at higher frequencies. This suggests that in the potential component, the power is concentrated in the acoustic resonant modes trapped in

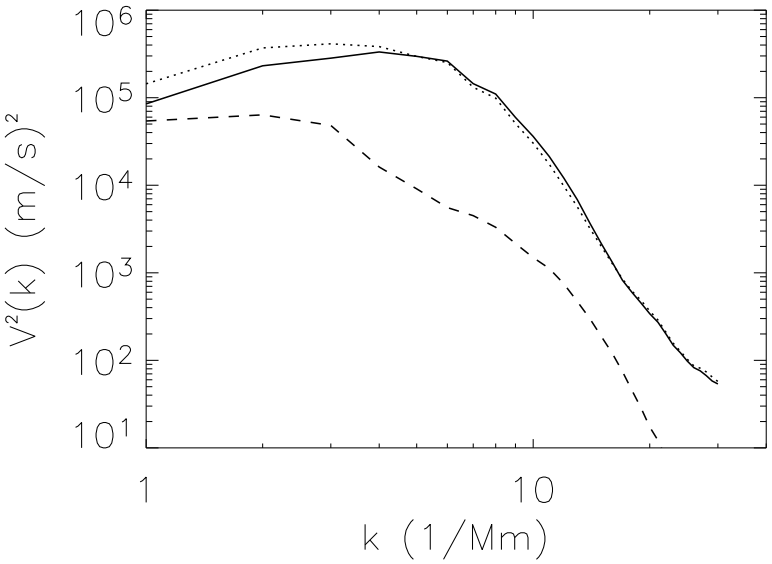

FIGURE 4. Spatial spectra of the total velocity squared (solid line) and its potential (dashed line) and rotational (dotted line) components. The energy content is much lower in the potential component, and its characteristic spatial scales are larger than for the rotational or total velocities.

the upper convection zone. We continue investigating the relationship between acoustics and turbulence in the simulated velocity fields, trying to address the problem of energy equipartition between turbulence and oscillations, and to understand the mechanism of generation of acoustic waves by stellar turbulence.

REFERENCES

ASPLUND, M., NORDLUND, Å., TRAMPEDACH, R., ALLENDE PRIETO, C. & STEIN, R. F. 2000a Line formation in solar granulation. I. Fe line shapes, shifts and asymmetries. *Astronomy & Astrophysics*, **359**, 729

ASPLUND, M., LUDWIG, H.-G., NORDLUND, Å., & STEIN, R. F. 2000b The effects of numerical resolution on hydrodynamical surface convection simulations and spectral line formation. *Astronomy & Astrophysics*, **359**, 669

BORUCKI, W. J., KOCH, D., BASRI, G., BROWN, T., CALDWELL, D., DEVORE, E., DUNHAM, E., GAUTIER, T., GEARY, J., GILLILAND, R., GOULD, A., HOWELL, S. & JENKINS, J. 2003 Kepler mission: a mission to find Earth-size planets in the habitable zone. *Proceedings of the conference on Towards other Earths: DARWIN/TPF and the search for extrasolar terrestrial planets, 22-25 April 2003, Heidelberg, Germany*

GEORGOBIANI, D., STEIN, R. F., NORDLUND, Å., KOSOVICHEV, A. G., & MANSOUR, N. N. 2004 High degree solar oscillations in 3D numerical simulations. *Proceedings of the SOHO14/GONG 2004 workshop "Helio- and asteroseismology: towards a golden future" from July 12-16 2004 at New Haven CT (USA)*

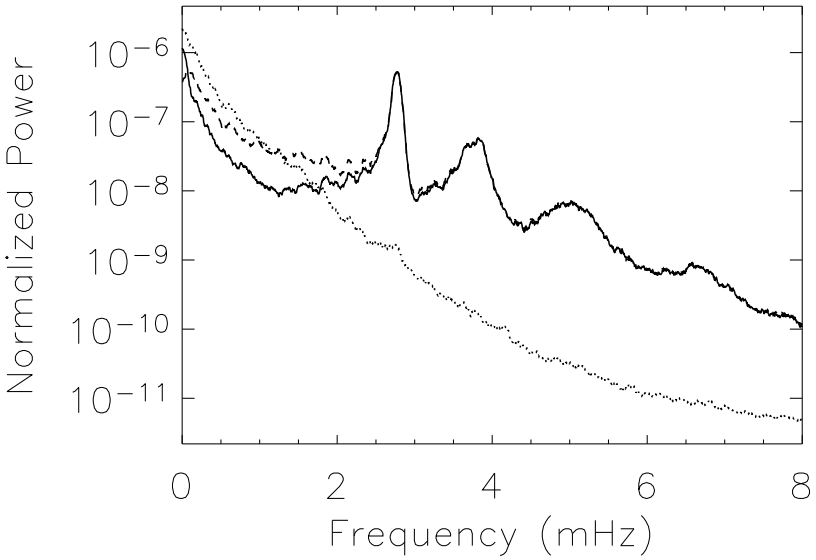

FIGURE 5. Non-radial power spectra of different velocity components. Total (solid line) and potential (dashed line) velocity show the oscillation mode peaks; they are very similar, except at low frequencies. Rotational (dotted line) velocity signal represents the background convective noise. The curves are smoothed over $\Delta\nu = 0.1$ mHz.

HILL, F., FISCHER, G., GRIER, J., LEIBACHER, J. W., JONES, H. B., JONES, P. P., KUPKE, R. & STEBBINS, R. T. 1994 The Global Oscillation Network Group site survey. 1: Data collection and analysis methods. *Solar Physics*, **152**, 321

NORDLUND, Å. & STEIN, R. F. 1990 3-D simulations of solar and stellar convection and magnetoconvection. *Computer Physics Communications*, **59**, 119

NORDLUND, Å. & STEIN, R. F. 2001 Solar oscillations and convection. I. Formalism for radial oscillations. *Astrophysical Journal*, **546**, 576

ROCA CORTES, T., MONTANES, P., PALLE, P. L., PEREZ HERNANDEZ, F., JIMENEZ, A., REGULO, C., & THE GOLF TEAM 1999 Low l solar p-mode oscillations parameters and convection. *ASP Conf. Ser. 173: Stellar structure: theory and test of convective energy transport*, 305

SCHERRER, P. H., BOGART, R. S., BUSH, R. I., HOEKSEMA, J. T., KOSOVICHEV, A. G., SCHOU, J., ROSENBERG, W., SPRINGER, L., TARBELL, T. D., TITLE, A., WOLFSON, C. J., ZAYER, I. & MDI ENGINEERING TEAM 1995 The Solar Oscillations Investigation - Michelson Doppler Imager. *Solar Physics*, **162**, 129

STEIN, R. F. & NORDLUND, Å. 2000 Realistic solar convection simulations. *Solar Physics*, **192**, 91

STEIN, R. F. & NORDLUND, Å. 2001 Solar oscillations and convection. II. Excitation of radial oscillations. *Astrophysical Journal*, **546**, 585